J Electroanal Chem, 162 (1984) 207–224
Elsevier Sequoia S.A., Lausanne – Printed in The Netherlands

THE ELECTROFORMATION AND ELECTROREDUCTION OF ANODIC FILMS FORMED ON SILVER IN 0.1 *M* SODIUM HYDROXIDE IN THE POTENTIAL RANGE OF THE Ag/Ag_2O COUPLE

M. LOPEZ TEIJELO *, J.R. VILCHE and A J. ARVÍA

Instituto de Investigaciones Fisicoquímicas Teóricas Aplicadas, INIFTA, Casilla de Correo 16, Sucursal 4, 1900 La Plata (Argentine)

(Received 9th June 1983)

ABSTRACT

The complex electrochemical reactions related to the electroformation and electroreduction of silver(I) oxide films in base electrolyte were investigated by means of combined potentiodynamic techniques and potential steps The anodic process involves the initial fast OH^- ion discharge yielding OH-adsorbed species and later continues to form the silver(I) oxide layer The latter behaves as a duplex structure anodic layer with a degree of hydration changing with depth The electroreduction characteristics of the anodic film depend both on potential sweep and anodic charge, and the relationships of the corresponding kinetic parameters fit qualitatively with those predicted by nucleation and growth mechanisms Activity increases of silver caused by the potential sweeps are interpreted by the simultaneous contribution of the increase in the concentration of silver active surface sites and the change in size distribution of silver electrodeposited from silver(I) oxide.

INTRODUCTION

The electrooxidation of silver to silver(I) oxide in base solutions has been extensively studied. The rate of the reaction increases with the applied potential but exhibits a peak value for an overpotential of 46 mV [1]. The galvanostatic electroreduction of silver oxide shows an appreciable cathodic overpotential [1–4]. The reaction from a clean silver surface initiates through the formation of AgOH species so that the $Ag/AgOH/OH^-$ couple is considered as the potential determining reaction for the reversible silver/silver oxide electrode [5]. As deduced for silver electrodes discontinuously scratched under potential control while immersed in 1 *M* KOH the formation of the first monolayer of silver(I) oxide is facilitated by an intermediate silver(I) species at monolayer coverage, which probably corresponds to AgOH [6]. The fast dissolution of silver as $Ag(OH)_2^-$ precedes phase formation on the electrode yielding a silver(I) oxide monolayer which thickens to form a dense multilayer [7,8].

* Present address. Departamento de Fisicoquímica, Facultad de Ciencias Químicas, Universidad Nacional de Córdoba, Sucursal 16, Casilla 61, 5016 Córdoba, Argentine.

0022-0728/84/$03 00

The formation of two distinct types of oxidized monolayer occurs in different potential ranges below the Ag/Ag_2O reversible potential [6]. Solid state diffusion, and nucleation and growth effects have already been pointed out as important in determining the potentiodynamic cathodic and anodic currents related to silver(I) oxide films [9–11]. A mechanism of nucleation of steps on the oxide surface has been suggested for the silver(I) oxide film formation under stirred conditions, including dissolution of silver followed by precipitation [8,12,13].

The electrochemical behaviour of polycrystalline silver was also investigated by different optical techniques. Thus, the electroreflexion values of silver in base indicate that, over a wide range of potentials, oxygen is adsorbed on silver in the form of OH groups, which between 0.5 V and 0.8 V incorporate into the metal lattice, through a process which involves no charge transfer [14]. Ellipsometric data also show an initial reversible oxygen adsorption [15,16], although the reactivity depends on the face of the single crystal [17]. Mathematical film formation models including the application of continuous mass and charge balance were used to explain time-dependent ellipsometric measurements of silver oxide films [18] in multidimensional space.

The effect of temperature on the electrochemical behaviour of silver in base solutions has recently been studied [19]. In the range $295\ K < T < 478\ K$ silver undergoes an active to passive transition. The corresponding potential shifts to less positive values and the passive current increases with increasing temperature [19].

The influence of light excitation in the oxidation and reduction of the Ag/Ag_2O electrode is also reported [20]. Light absorption by silver(I) oxide yields silver(II) oxide. Primary and secondary photoeffects were found [10]. Raman spectroscopy is capable of monitoring the photo-electrochemical generation of silver(II) oxide from silver(I) oxide [21].

Despite the fact that the conclusions from the many investigations of the subject [9–13,19–25] suggest that previously proposed mechanisms for the oxidation-reduction behaviour of silver in alkaline solutions are viable, there are still important questions unanswered, which mainly relate to the structure of the different oxides and hydroxides and contributions of possible chemical transformations in the electrochemical reaction, as is revealed by the complex potentiodynamic response of silver in base electrolytes in the potential range of the $Ag/Ag_2O/OH^-$ couple [26]. The present work attempts both to throw further light on the distinct types of oxide layers formed during the electrooxidation of silver to silver(I) oxide, as revealed by electrochemical techniques and to indicate the controlled potential condition required for comparative structural studies using optical methods [20].

EXPERIMENTAL

The experimental set-up is the same as that described in a previous publication [26]. "Specpure" silver wires (0.5 mm diameter) were used as working electrodes in 0.1 *M* NaOH, in a purified N_2 gas saturated atmosphere at 25°C. Silver electrodes were mechanically polished with 400 and 600 grits alumina–acetone suspensions,

diamond paste, and then thoroughly rinsed in triple-distilled water. Potentials were measured using a SCE but in the text they are referred to the NHE scale.

After a cathodization for 5 min in the hydrogen evolution potential region, the following potential perturbation programmes were applied: single (STPS) and repetitive (RTPS) triangular potential sweeps both in symmetric and asymmetric profiles, between preset cathodic ($E_{s,c}$) and anodic ($E_{s,a}$) switching potentials at a scan rate (v), combined potential/time functions in order to promote either the potentiostatic or the potentiodynamic ageing effects of the electroformed surface species, and intermediate potential steps included in potentiodynamic perturbation programmes. Single and combined potentiostatic steps were also applied to the working electrode. The scheme of the complex potential/time (E/t) perturbations are depicted in the corresponding figures. Conventional electronic instrumentation was used for this purpose.

RESULTS

The conventional RTPS i/E potentiodynamic profile, run at 0.01 V/s between $E_{s,c} = 0.05$ V and $E_{s,a} = 1.15$ V, exhibits four anodic current peaks (I, II, III and IV) during the positive going potential scan, the returning scan shows two cathodic current peaks (V and VI) (Fig. 1). The description of this voltammogram, which is shown for the sake of comparison, has already been made [17]. Peaks I, II and III are related to the electroformation of Ag(I) + oxygen-containing species and peak IV corresponds to the electroformation of silver(II) oxide.

The location and shape of the electroreduction profile depends remarkably on $E_{s,a}$. Thus, once the stabilized RTPS has been attained within the Ag(0)/Ag(I) couple potential range (Fig. 2), the stepwise decrease of $E_{s,a}$ produces net changes in the electroreduction profiles which depend on whether $E_{s,a}$ lies in the potential range of peak III (Fig. 2a), II (Fig. 2b) or I (Fig. 2c). When $E_{s,a}$ is within the potential

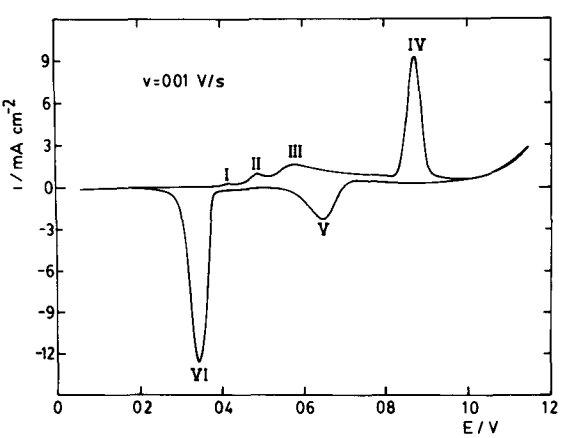

Fig. 1. Stabilized RTPS E/i display run at 0.01 V/s

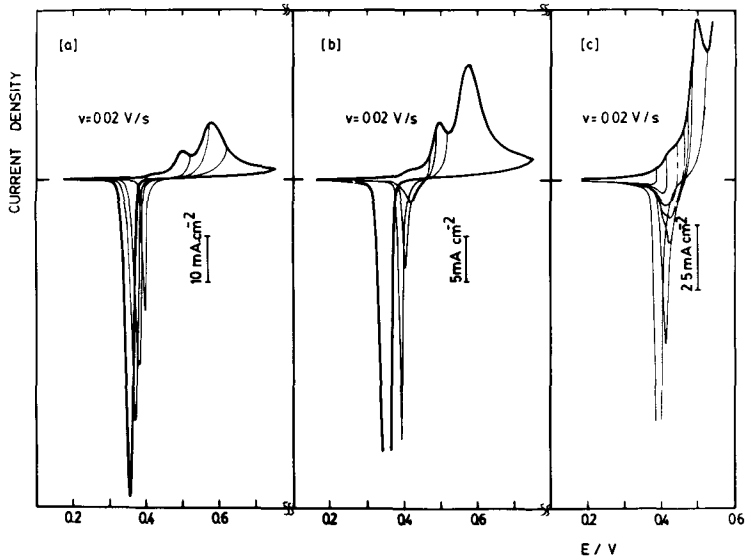

Fig 2 Influence of $E_{s,a}$ on the E/i profiles recorded with RTPS at 0.02 V/s

range of peak I, the electroreduction profile is highly reversible, the lower $E_{s,a}$ the greater the reversibility of the system. In this case, under certain conditions a net splitting of peak VI can be observed. When $E_{s,a}$ lies in the potential range of peaks II and III, the potential of peak VI becomes more positive as $E_{s,a}$ progressively decreases, however, when $E_{s,a}$ lies in the potential range of peak II the potential shift

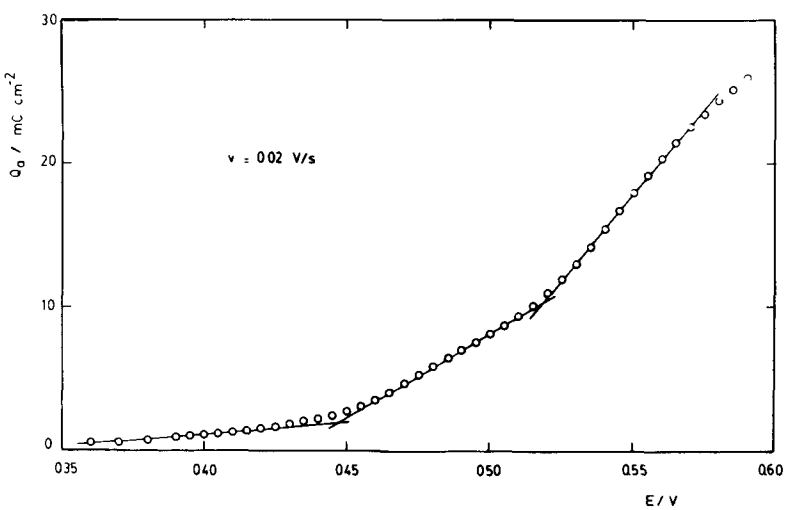

Fig. 3 Dependence of Q_a on E at $v = 0.02$ V/s

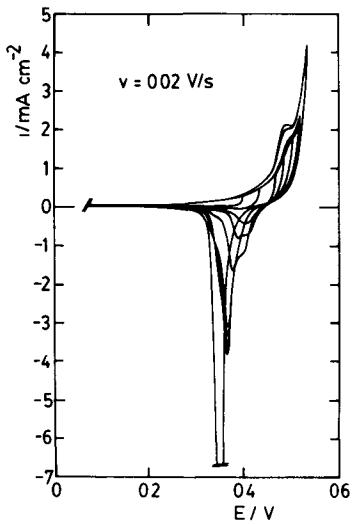

Fig. 4 RTPS E/i displays obtained by increasing progressively $E_{s,a}$ after four potential cycles in each limited potential region $E_{s,c} = -0.1$ V $v = 0.02$ V/s

of peak VI is remarkably more sensitive to $E_{s,a}$ than when the latter is within the potential range of peak III. In principle, the greater $E_{s,a}$ the sharper the contour of peak VI and the larger both the anodic (Q_a) and the cathodic (Q_c) charges involved, although the Q_a/Q_c charge ratio is, however, always close to one.

The Q_a vs. E plot related to the Ag(I)-species electroformation (Fig. 3) shows at

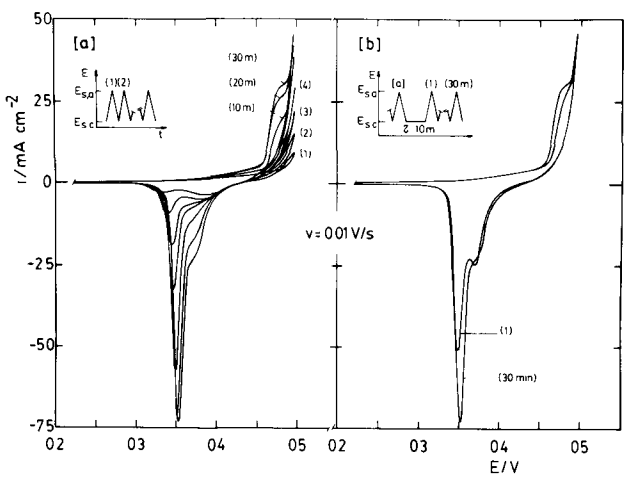

Fig 5. Potentiodynamic E/i curves at $v = 0.01$ V/s run between $E_{s,c} = 0$ V and $E_{s,a} = 0.5$ V (a) 1st to 4th cycles and those after 10 min, 20 min and 30 min are depicted (b) 1st and nth cycles after 10 min potential holding at $E_{s,c}$ are shown.

least two breaks and three well-defined regions which can be interpreted as linear Q_a vs. E relationships. Each straightline portion is associated with one anodic current peak in the i/E potentiodynamic profile.

The multiplicity of peak VI can be more easily seen either by a progressive increase of $E_{s,a}$ during the RTPS or by applying the combined potential perturbation programmes. In the first case (Fig. 4) a fresh polished electrode which has been previously cathodized in the hydrogen evolution potential range is used, $E_{s,c}$ is initially set at -0.1 V and $E_{s,a}$ at 0.4 V and then the RTPS including the stepwise increase of $E_{s,a}$ within the potential range of peaks I and II is applied. The i/E curves shown in Fig. 4 correspond to the four first RTPS cycles at each $E_{s,a}$. They change considerably during cycling only when $E_{s,a} > 0.5$ V. Thus, as Q_a increases, peak II becomes better defined and the charge distribution among the various cathodic processes is modified. A similar complex behaviour is observed after a prolonged RTPS by proper adjustment of $E_{s,a}$ just at the beginning of the RTPS (Fig. 5a). Furthermore, the potentiodynamic i/E profiles run with freshly polished electrodes show a rapid and progressive activation of the electrooxidation process during the RTPS until the stabilized i/E profile already seen is attained. It should be noticed that both peak multiplicity and activation effects depend considerably on $E_{s,a}$, $E_{s,c}$ and v. The same stabilized i/E contour results when the RTPS involves the potential holding at $E_{s,c}$ (Fig. 5b). Otherwise, both the peak multiplicity and the cathodic charge transferred during the negative going potential excursion depend strongly on both E_τ and τ when E_τ is within the potential range of peaks I and II (Fig. 6).

The anodic film resulting under these potentiodynamic conditions behaves as a mixture of various species with residual reactivity. This can be concluded from the

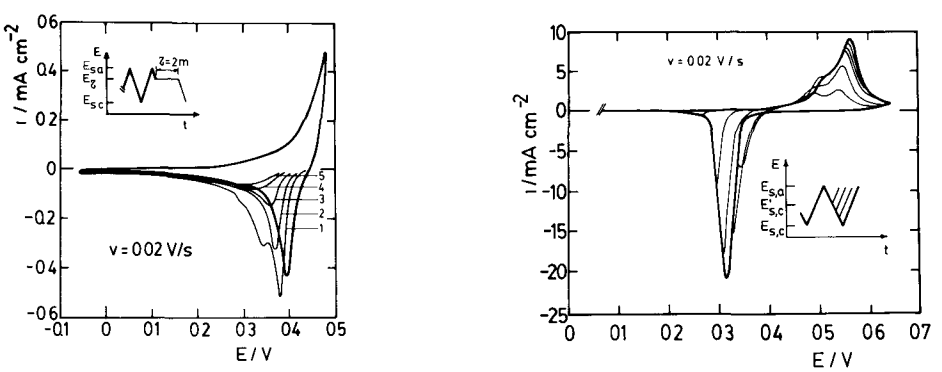

Fig 6 Influence of potential holding at E_τ during $\tau = 2$ min on the cathodic RTPS after attaining the stabilized RTPS E/i contour. $v = 0.02$ V/s, $E_{s,c} = -0.06$ V and $E_{s,a} = 0.48$ V $E_\tau = 0.439$ V, profile 1, $E_\tau = 0.421$ V, profile 2, $E_\tau = 0.406$ V, profile 3, $E_\tau = 0.393$ V, profile 4, $E_\tau = 0.378$ V, profile 5

Fig. 7 Influence of $E'_{s,c}$ on the E/i profiles recorded at 0.02 V/s, after the stabilized RTPS E/i display between $E_{s,c} = -0.16$ V and $E_{s,a} = 0.64$ V had been attained

electroreduction of different fractions of the anodic film, using for this purpose the perturbation programme depicted in Fig. 7. The contribution of the electrooxidation process taking place in the potential region of peak III diminishes only when a fraction less than one half of the anodic layer is electroreduced. In this case, by reversing the potential sweep before the cathodic current peak potential, $E_{p,c}$, is reached, an increase of anodic current in the following positive going potential excursion is observed which indicates an activation of the electrooxidation process.

The i/E profile resulting from the combined RTPS perturbation programme (Fig. 8) within the potential limits of peaks I and III exhibits two well defined cathodic current contributions in peak VI, their relative charge depending remarkably on $E'_{s,c}$. A comparable effect is observed when the positive going potential sweep includes a step in the potential range of peak II (Fig. 9). In this case, the overall electroreduction profile, which moves towards negative potentials, exhibits also a cathodic peak splitting although less clearly seen than in Fig. 8. The influence of E_τ is comparatively much smaller than that of $E'_{s,c}$.

The sharp cathodic pseudocapacitance/potential peaks (Fig. 10) obtained under RTPS with $v_a = v_c$ show the appreciable increase in the pseudocapacitance associated with the electroreduction process as v decreases. Simultaneously, the potential of the

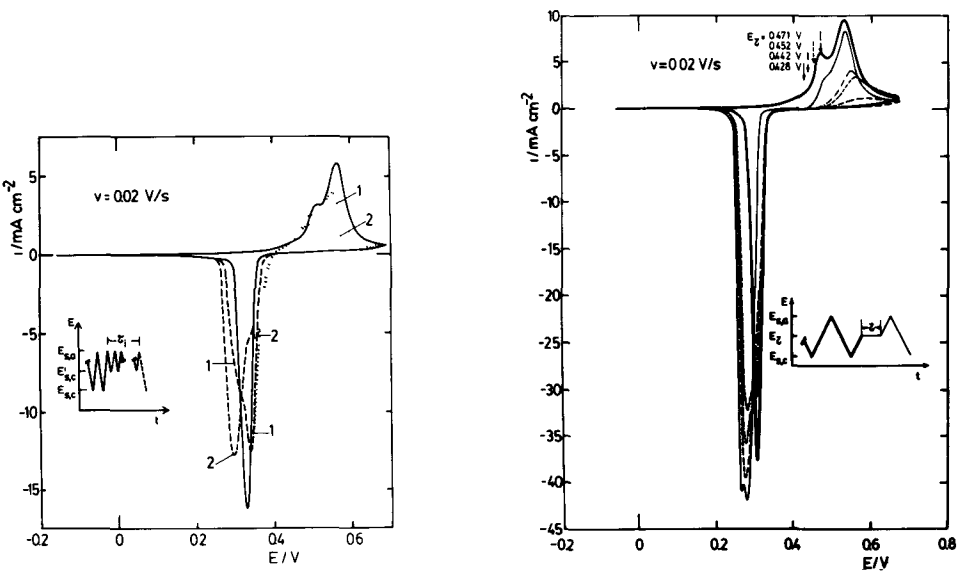

Fig 8 Potentiodynamic E/i displays obtained with the perturbation programme depicted in the figure The full trace corresponds to the stabilized RTPS E/i profile and the dashed traces correspond to the potentiodynamic ageing. $v = 0\,02$ V/s; $E_{s,c} = -0.16$ V, $E_{s\,a} = 0\,68$ V, $\tau_1 = \tau_2 = 5$ min; $(E'_{s,c})_1 = 0\,335$ V, $(E'_{s\,c})_2 = 0\,355$ V

Fig. 9. Influence of the potential holding at E_τ during $\tau = 10$ min on the potentiodynamic E/i profiles obtained with the perturbation programme depicted in the figure $v = 0\,02$ V/s

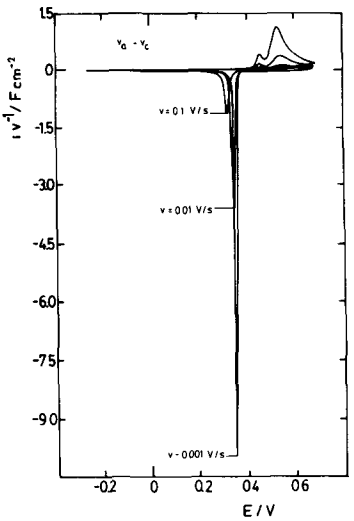

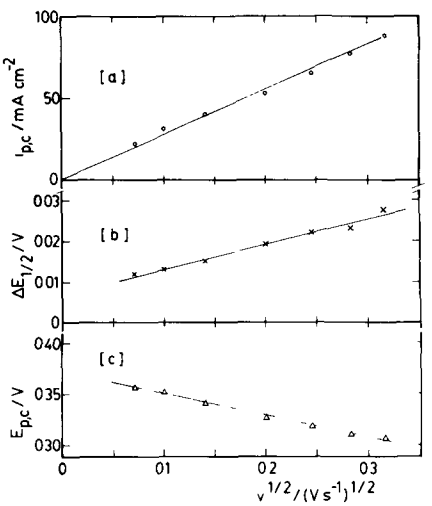

Fig. 10 $i\ v^{-1}$ vs E plots resulting at different sweep rates under RTPS conditions $v_a = v_c$

Fig. 11 Dependence of (a) $i_{p,c}$, (b) $\Delta E_{1/2}$ and (c) $E_{p,c}$ on $v^{1/2}$ derived from the RTPS measurements of the type described in Fig 10

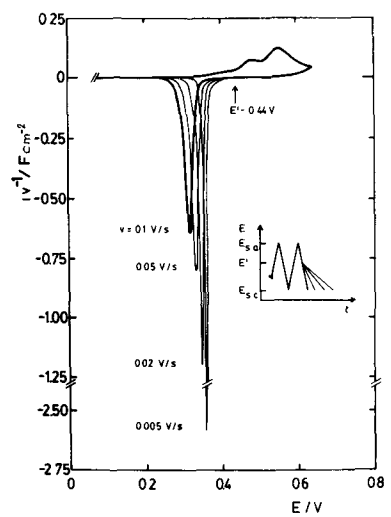

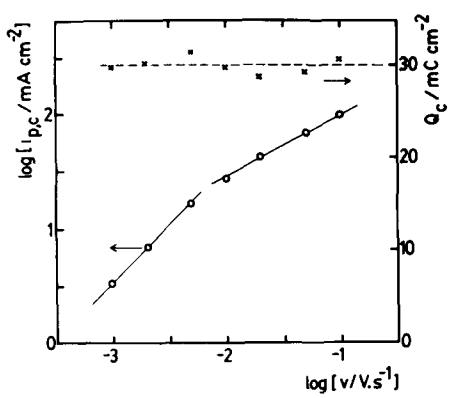

Fig. 12 Influence of v_c on the electroreduction $E/i \cdot v^{-1}$ profile after attaining the stabilized E/i contour according to the potential programme depicted in the figure $v = 0.1$ V/s; $E_{s,c} = -0.26$ V; $E_{s,a} = 0.64$ V; $E' = 0.44$ V

Fig. 13. Dependence of $i_{p,c}$ and Q_c on v_c derived from data shown in Fig. 12

pseudocapacitance peak becomes more positive for decreasing v values. This correlates with the fact that the overall charge increases as v decreases. This means that an oxide film of a greater average thickness is electroformed and electroreduced as v decreases. For the cathodic peak resulting under stabilized RTPS conditions, the peak potential ($E_{p,c}$), half-peak width ($\Delta E_{1/2}$) and peak height ($\iota_{p,c}$) change linearly with $v^{1/2}$ (Fig. 11). From the RTPS ι/E displays run at $v_a = v_c$ within preset $E_{s,c}$ and $E_{s,a}$ values, both Q_a and Q_c exhibit a linear dependence with $v^{-1/2}$. The ratio Q_a/Q_c is close to one, and Q_∞, the charge extrapolated as $v \to \infty$, is $Q_\infty = 15$ mC/cm^2.

The cathodic pseudocapacitance/potential profile at different v_c under constant Q_a run after the stabilized RTPS ι/E profile at 0.1 V/s was attained, was studied by changing v_c at $E' = 0.44$ V, the potential at which for a fixed $E_{s,a}$ the net current is null. At this potential the formation of the film has already finished (Fig. 12). The pseudocapacitance peak becomes sharper and its potential more positive as v diminishes. These results indicate that the potential for electroreducing the anodic film is conditioned by the time the system is allowed for reaction. From runs made at constant Q_c, the log $\iota_{p,c}$ vs. log v plot exhibits two straight-line portions (Fig. 13), one with the slope equal to 1 ($v_c < 0.01$ V/s) and another with the slope equal to 0.5 ($v_c > 0.01$ V/s). On the other hand $\Delta E_{1/2}$ decreases with v_c, tending to a value ca. 4–5 mV at low v_c values. These results suggest a drastic change in the mechanism of the electroreduction process.

The electroreduction profiles resulting from the potential perturbation programme depicted in Fig. 12, that is from stabilized ι/E profiles, obtained at low

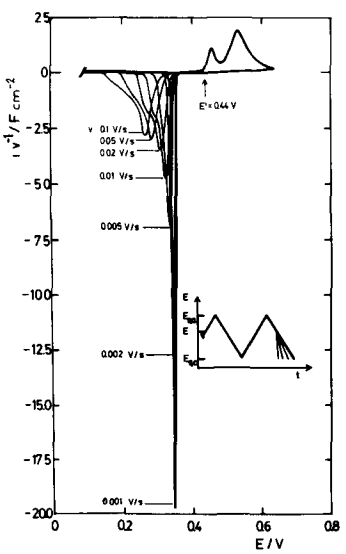

Fig. 14. Influence of v_c on the electroreduction E/ι v^{-1} profile after attaining the stabilized E/ι contour according to the potential programme depicted in the figure $v = 0.001$ V/s, $E_{s,c} = -0.26$ V, $E_{s,a} = 0.64$ V, $E' = 0.44$ V

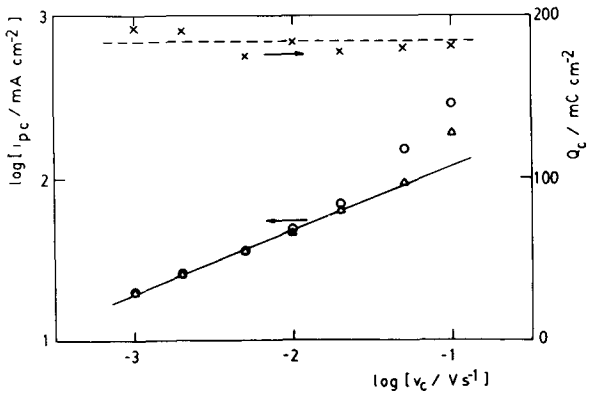

Fig. 15. $\log i_{p,c}$ vs $\log v_c$ and Q_c vs. $\log v_c$ plots derived from the data shown in Fig 14, with (△) and without (○) correction for the cathodic current due to the hump at the negative potential side

values of v_c, depend also on the value of v_a used for the anodic film electroformation. Thus, at $v_a = 1$ mV/s (Fig. 14) the electroreduction profile reveals two overlapping current contributions, which are more clearly noticed at large v_c. The value of Q_c associated with the anodic film electroformed at 1 mV/s is greater than that of the film electrogenerated at 0.1 V/s. For a constant $Q_a = Q_c$ (Fig. 15) the $\log i_{p,c}$ vs. $\log v_c$ plot can be interpreted in the low v range as a straight line with a slope of

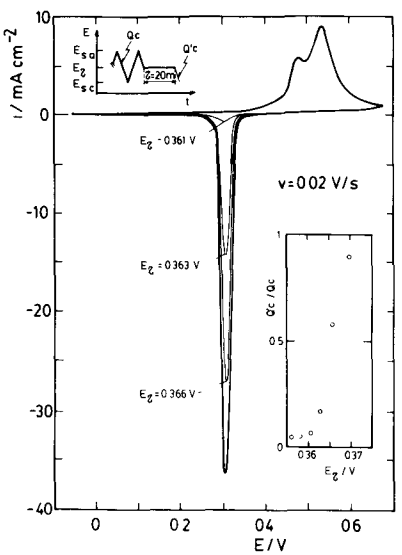

Fig. 16 Potentiodynamic E/i displays obtained with the perturbation programme depicted in the figure Q_c corresponds to the total cathodic charge recorded under stabilized RTPS conditions and Q_c' corresponds to the cathodic charge recorded after a potential holding at E_τ during $\tau = 20$ min $v = 0\,02$ V/s

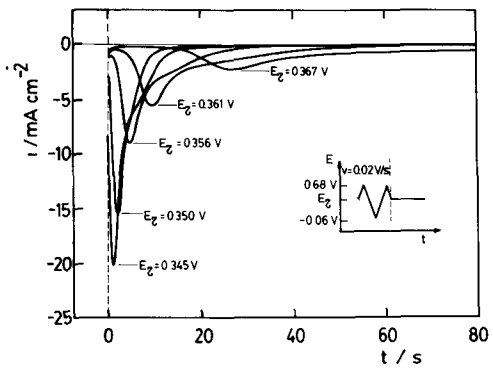

Fig. 17. Cathodic current transients recorded during the potential holding at $E_\tau = 0.345$ V, profile 1; $E_\tau = 0\ 350$ V, profile 2, $E_\tau = 0.356$ V, profile 3, $E_\tau = 0\ 361$ V, profile 4, $E_\tau = 0\ 367$ V, profile 5

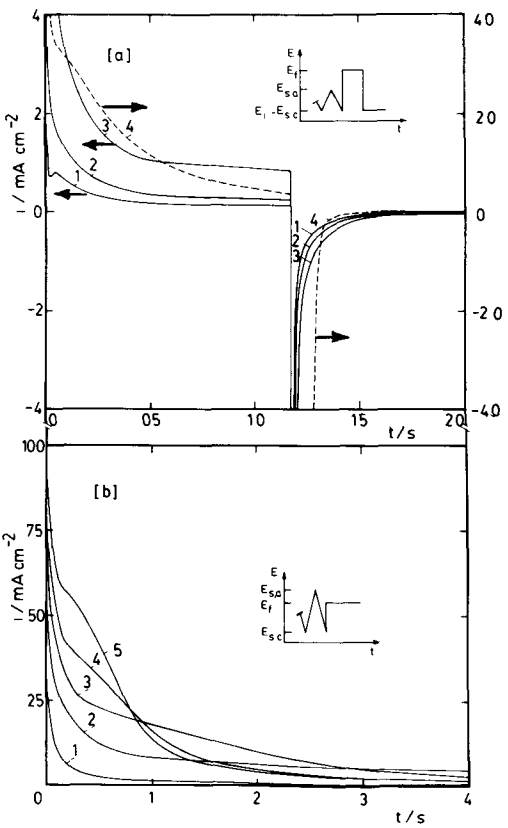

Fig 18. (a) Current transients run after the stabilized E/i RTPS contour at $v = 0.02$ V/s between $E_{s,c} = -0.06$ V and $E_{s,a} = 0.385$ V had been attained $E_f = 0.411$ V, curve 1, $E_f = 0\ 443$ V, curve 2, $E_f = 0\ 485$ V, curve 3, $E_f = 0.544$ V, curve 4. (b) Anodic current transients recorded as indicated above under the following conditions: $E_{s,c} = -0.06$ V and $E_{s,a} = 0.74$ V $E_f = 0\ 449$ V, curve 1, $E_f = 0\ 528$ V, curve 2; $E_f = 0\ 580$ V, curve 3, $E_f = 0.633$ V, curve 4; $E_f = 0.686$ V, curve 5

about 0.4 ($v < 0.05$ V/s). The cathodic charge contribution at negative potentials from that of peak IV, is more remarkable as v_c increases. This makes the evaluation of data from the log $i_{p,c}$ vs. log v plot at $v_c > 50$ mV/s rather uncertain.

Runs made by holding the potential at E_τ in the potential range of peak I after the stabilized RTPS i/E profile has been attained, show that the electroreduction charge (Q'_c) decreases remarkably. The potential perturbation programme used in these cases produces the accumulation of products at E_τ. For a constant potential holding time ($\tau = 20$ min), the charge decrease is considerably dependent on E_τ (Fig. 16). The dependence of the Q'_c/Q_c ratio on E_τ changes abruptly from $\simeq 0.05$ for $E_\tau < 0.36$ V to $\simeq 1.0$ for $E_\tau > 0.37$ V. The inflexion point which corresponds practically to $Q'_c/Q_c = 0.5$, occurs at $E_\tau = 0.365$ V. The current transients associated with the potential holding depend on the E_τ value (Fig. 17). In the 0.340 V $< E_\tau <$ 0.362 V range, two different contributions are seen during the electroreduction process, the first one appearing at the lowest potential (0.345 V) as a sharp current maximum which decays very rapidly. The second contribution progressively overlaps with the former as E_τ becomes more positive. When $E_\tau > 0.37$ V, a current decrease is recorded during the time τ, not a peak.

The potential steps starting from $E_{s,c}$ were also successively applied to the electrode after the stabilized RTPS i/E profile, as depicted in Fig. 4, had been obtained. The values of the potential steps (E_f) were adjusted to record the anodic transients starting from $E_{s,c}$. In this case the anodic film formation occurs on the electroreduced silver surface (Fig. 18a). The anodic current transients at 0.390 V $< E_f < 0.415$ V exhibit a net maximum at ca. 50 ms, which is no longer observed at $E_f > 0.420$ V, probably because it becomes smaller as E_f increases. On the other hand, when $E_f > 0.53$ V, a second current maximum appears at ca. 0.10–0.15 s. In all these cases the corresponding electroreduction profiles show a continuous current decay which is more extended according to the amount of anodic film. A similar behaviour for the anodic film growth is obtained when the initial stabilized RTPS i/E profile covers the potential range of the Ag(0)/Ag(I) couple (Fig. 18b). In this case the current transient changes when $E_f > 0.53$ V.

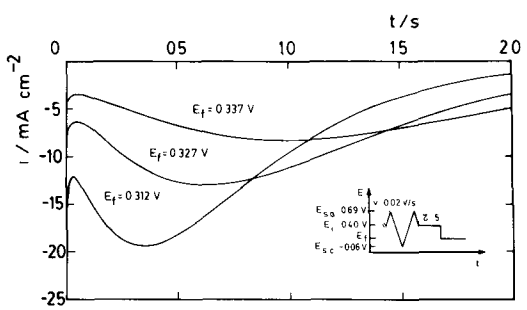

Fig. 19 Cathodic current transients at E_f after a potential holding at $E_i = 0.40$ V during $\tau = 5$ min $v = 0.02$ V/s, $E_{s,c} = -0\,06$ V and $E_{s,a} = 0\,69$ V.

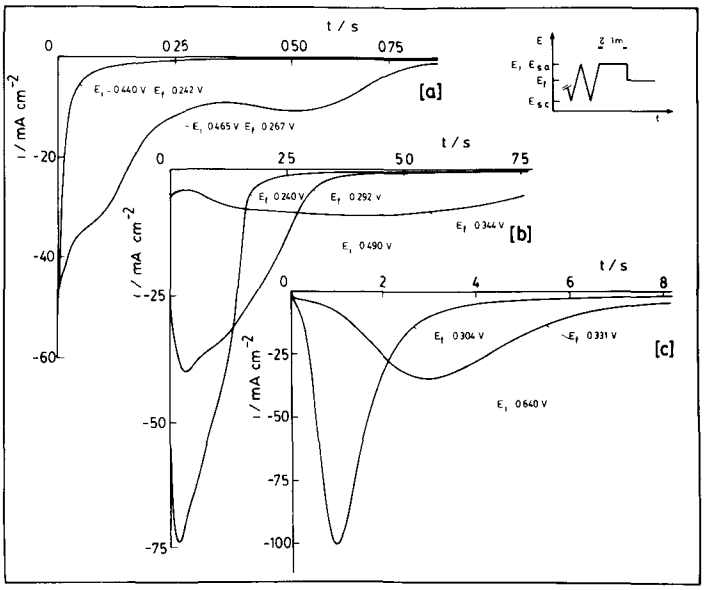

Fig 20 Cathodic current transients recorded at E_f after a potential holding at $E_i = E_{s,a}$ during $\tau = 1$ min, varying at convenience both E_i and E_f The electrode had been previously cycled at 0 02 V/s between $E_{s,c} = 0$ V and different $E_{s,a}$ values

The cathodic current transients give further information about the electroreduction process when the anodic film is firstly held at E_i for $\tau = 5$ min, and later electroreduced at an E_f value which is negative with respect to E_i (Fig. 19). When the electrode is first held at $E_{s,a} = E_i$ for a time, $\tau = 1$ min, before stepping the potential to E_f (Fig. 20), so that a reactant with the same history becomes available for electroreduction, the corresponding current transient involves increasing charges as E_i approaches 0.5 V, but when this potential is exceeded the current transient shows two distinct processes associated with a constant charge value. This indicates that the electroreduction follows different reaction patterns according to E_i.

DISCUSSION

For the discussion of results it is convenient to present them orderly in the following way:

(i) The anodic film in the potential range of silver(I) is constituted of at least three different species which are formed in well defined potential ranges (Figs. 1–3).

(ii) The product formed in the first stage, corresponding to OH-containing surface species [5,6,20,26] results from a reversible electrochemical reaction.

(iii) The products from the second and third stages probably correspond to differently hydrated silver(I) oxides. These products participate in phase reactions

related to ageing of the anodic film as seen from the corresponding changes in the electroreduction i/E profiles of the anodic film (Figs. 6 and 8).

(iv) At a fixed potential, or under open circuit conditions, the anodic film also partially dissolves in the electrolyte [7,8].

(v) During the potential cycling for $E_{s,a} > 0.5$ V there is a charge increase playing a part in the overall process which can be primarily related to an increase in the surface roughness due to the base metal electrooxidation process.

(vi) The freshly electroreduced silver within the surface film appears to be more reactive than the initial polycrystalline material (Figs. 7 and 8). This should contribute to the anodic current enhancement during the potential cycling through an increase in the number of active sites for the metal attack.

(vii) The kinetics of the anodic film electroformation under either a potential sweep (Fig. 9) or a potential step (Fig. 18) depend on both the potential and the amount of anodic product already present at the electrode.

(viii) For the same amount and history of anodic film the electroreduction kinetics depend on whether the value of the potential step falls within the 0.240 V–0.350 V range or within the 0.355 V–0.380 V range (Fig. 20).

(ix) For a constant, but small ($Q_a < 30$ mC/cm^2) anodic charge, two different relationships between the kinetic parameters are found depending on whether v is greater or less than 10 mV/s (Fig. 13).

(x) For a constant but relatively large anodic charge ($Q_a > 100$ mC/cm^2) there is a single reliable relationship between $i_{p,c}$ and v_c which is distinct from those indicated in (ix) (Fig. 15).

Therefore, the anodic film formation on silver in base solution in the potential range of the Ag(0)/Ag(I) redox couple is a process which is very complex both in the nature of the various products and in the change of the electroreduction kinetics for the same anodic film according to the potential applied to the electrode.

Some aspects of the overall processes, despite their great complexity, can be discussed through general phenomenological models which neglect detailed structural features. The present results can be, in principle, only qualitatively related to the composite multilayer model proposed to explain the ellipsometric response of galvanostatically formed anodic films on silver in alkaline solution [18], because of the different history of the silver oxide films. On the basis of previous electrochemical data [16,26] and optical results [15,16,18], the initial stage of anodic film formation should comprise the discharge of OH^- ion in contact with silver, probably through ionic specific adsorption, yielding a metal surface covered by the OH species. This reaction can be formally represented as:

$$Ag^* + OH^- = Ag(OH)_{ad} + e^- \quad (1)$$

where the asterisk denotes a reactive site at the electrode surface. This type of reaction appears as the first reversible underpotential step in the electrodissolution and passivation of most metals in base aqueous electrolytes [27–35]. The following stages correspond to multilayer anodic growth in the form of at least two species of hydrated structurally different silver oxide. In this sense, the $Ag(OH)_{ad}$ species

becomes a reaction intermediate in the overall process lying in a plane in contact with the metal moving inwards as the anodic reaction proceeds. This process can be represented as follows:

$$|Ag_x|Ag(OH)_{ad} + 2\ OH^- + y\ H_2O = |Ag_{x-2}|Ag(OH)_{ad}/Ag_2O \cdot (y+1)\ H_2O + 2\ e^- \quad (2)$$

where $Ag_2O \cdot (y+1)\ H_2O$ = layer I, so that the electrode at the initial stages of the multilayer formation can be given by a duplex structure such as $Ag/Ag(OH)_{ad}/Ag_2O \cdot (y+1)\ H_2O$, that is metal/monolayer/layer I. Then, after layer I acquires a certain thickness which is difficult to evaluate because of the change in the film density caused by the gradient in the water content of the hydrated oxide and hydroxide species, the multilayer growth continues to produce layer II, which should comprise, as suggested from ellipsometric data [18,36] a structure more compact (less hydration) than that of layer I. The overall reaction may be written as:

$$|Ag_x|/\text{layer I} + 2\ (OH^-)_{ext} + y'\ H_2O = |Ag_{x'-2}|/\text{layer I/layer II} + 2\ e^- \quad (3)$$

where $x' < x$ and $y' < y$ and layer II = $Ag_2O \cdot (y'+1)\ H_2O$. Then, the structure of the electrode becomes more complex and it can be represented either as Ag/monolayer/layer I/layer II or as Ag/layer I/layer II since the thickness of the inner monolayer at this stage becomes negligible.

The structures of both layer I and layer II participate in ageing processes as revealed by the characteristics of the potentiodynamic electroreduction profile which, under a constant charge condition, moves towards more negative potentials on increasing the lapse of time between the anodic film formation and its electrodissolution [26].

Finally, the anodic reaction is further complicated by the possible chemical dissolution of the film [7,8], a reaction which is favoured in base solutions by the following equilibria:

$$Ag_2O + 2\ OH^- = 2\ AgO^- + H_2O \quad (4a)$$

$$Ag_2O + H_2O = 2\ AgO^- + 2\ H^+ \quad (4b)$$

The equilibrium concentration of reaction (4a) is $\log[AgO^-] = -17.72 + pH$ for nonhydrated oxide, and $\log[AgO^-] = -12.10 + pH$ for hydrated oxide at 25°C [25]. In base solutions, the experimental equilibrium data for reaction (4b) show a minimum solubility of Ag_2O at a pH 12.2. Beyond this pH the solubility increases linearly with pH up to pH 14 [36]. According to Pound et al. [19] at 298 K the solubility of Ag_2O is 1.9×10^{-6} mol kg^{-1} at pH 12 and 9.4×10^{-5} mol kg^{-1} at pH 14.

Under potentiodynamic conditions, the cathodic process implies kinetics which depend on the amount of anodic film and on the potential sweep rate. Apparently, the cathodic process can be associated with different nucleation and growth-type mechanisms as earlier suggested by various authors [9–13]. Recent advances in formulating nucleation and growth mechanisms [37] allow the analysis of the present

results in terms of two limiting situations, that is for a small and for a large anodic charge related to the oxide layer. For the former case, $Q_a < 30$ mC/cm^2, (Fig. 13) at low v ($v \to 0$) the linear relationships i_p vs. v; $E_p \simeq$ constant and $\Delta E_{1/2} \to 0$ (very sharp electroreduction peak) suggest that the electrode reaction follows a progressive nucleation and growth mechanism [37], probably involving nucleation sites at the oxide covered base metal where silver atoms are electrodeposited during the process. In this case, at large v ($v \to \infty$), a i_p vs. $v^{1/2}$ relationship should be approached. Unfortunately, the results obtained for $Q_a > 30$ mC/cm^2 cannot be as straightforwardly analysed as those for small Q_a values because of the multiplicity of the electroreduction profile, which may involve a partial diffusion controlled electroreduction, with either a simple, or with an additional variable, ohmic polarization contribution cause to a great extent by the lack of hydration equilibrium during the fast potentiodynamic sweep. On the other hand, when the charge involved in the electroformation of the anodic film is large ($Q_a \simeq 200$ mC/cm^2) the kinetic relationship both at low and at high v satisfied the predictions of the instantaneous nucleation and growth model [18], although at high v the interpretation of results becomes again rather uncertain because of the multiplicity of the electroreduction current peak. The peak multiplicity also suggests that at large sweep rates layers I and II electroreduce independently. The characteristics of the current transients run at constant potential steps agree with the predictions of nucleation and growth mechanism [37] for the electroreduction of the silver oxide anodic film.

Finally, the apparent increase in surface roughness should be mainly attributed to two different but intermingled effects. One is the increase in the concentration of surface active sites (Ag*) and the other corresponds to the size distribution of electrodeposited silver, both produced by the electroreduction of the anodic film. Recent results both from Raman enhancement [21,38] and increase in the electrochemical reactivity of the hydrogen evolution reaction of silver electrodes after drastic potential perturbation [39] seem to confirm the importance of these two contributions in defining the activity of silver and other metal electrodes such as Au [28] and Cu [40] in acid and base electrolytes.

CONCLUSIONS

The present results confirm that the electrooxidation of silver to silver(I) oxide is a complex process which initiates through the fast discharge of OH^- ion yielding OH-adsorbed species. The growth of the anodic film furnishes a multilayered structure which can be at least a duplex-type film that consists of two distinct types of silver(I) oxide layers. The structural difference of each layer is, in principle, associated with a decrease in depth as the water content in the film changes, in agreement with recent ellipsometric results [41]. In this sense, due to ageing effects a controlled history of the anodic film becomes an important requirement for the general validity of conclusions from optical measurements. Time dependent ellipsometric measurements of silver oxide films in base solutions have already been reported [18].

The electroreduction of the anodic film follows apparently the nucleation and growth mechanism as previously pointed out for both the anodic and the cathodic processes related to silver(I) oxide films.

Finally, the increase in electrochemical activity of silver caused by the different potential perturbations are explained through the increase in the concentration of silver active sites at the metal surface and the change in size distribution of silver electrodeposited from silver(I) oxide.

ACKNOWLEDGEMENTS

INIFTA is sponsored by the Consejo Nacional de Investigaciones Científicas y Técnicas, the Universidad Nacional de La Plata and the Comisión de Investigaciones Científicas (Provincia de Buenos Aires).

One of us (M.L.T.) thanks the University of Córdoba for leave of absence.

REFERENCES

1 G T Croft, J. Electrochem. Soc , 106 (1959) 278
2 R. Glicksman and C K. Morehouse, J. Electrochem Soc., 104 (1957) 599
3 S A. Rozentsveig, B.V. Ershler, E L Shtrum and M M. Ostanina, Tr Soveshch. Elektrokhim. 4th, 1950 (1953) 571.
4 Z Takehara, Y Namba and S Yoshizawa, Electrochim Acta, 13 (1968) 1395
5 P Stonehart, Electrochim. Acta, 13 (1968) 1789
6 G.T Burstein and R.C Newman, Electrochim Acta, 25 (1980) 1009
7 R D. Giles, J A Harrison and H R Thirsk, J Electroanal Chem , 22 (1969) 375
8 J Ambrose and R.G Barradas, Electrochim. Acta, 19 (1974) 781
9 B.V Tilak, R.S. Perkins, H. Angerstein-Kozlowska and B E Conway, Electrochim Acta, 17 (1972) 1447.
10 R.S Perkins, B.V Tilak, B E Conway and H. Angerstein-Kozlowska, Electrochim Acta, 17 (1972) 1471.
11 J.M M Droog and T Huisman, J Electroanal Chem , 115 (1980) 211
12 D.B. Gibbs, B. Rao, R A Griffin and M T Dignam, J Electrochem Soc , 122 (1975) 1167
13 B Miller, J Electrochem Soc , 117 (1970) 491.
14 E.B. Brick, R M Lazorenko-Manevich and Ya.M Kolotyrkin, Elektrokhimiya, 13 (1977) 1520
15 Z.I Kudryavtseva, V A Openkin, N A. Zhuchkova and N A Shumilova, Elektrokhimiya, 14 (1978) 517.
16 J M M. Droog, P.T Alderliesten and G.A. Bootsma, J Electroanal. Chem , 99 (1979) 173.
17 J M.M. Droog, J. Electroanal. Chem., 115 (1980) 225
18 R H. Muller and C.G Smith, Surf. Sci., 96 (1980) 375.
19 B.G. Pound, D D. Macdonald and J.W. Tomlinson, Electrochim. Acta, 24 (1979) 929, 25 (1980) 563, 1293.
20 R. Memming, F. Mollers and G. Neumann, J Electrochem Soc , 117 (1970) 451
21 R. Kotz and E. Yeager, J Electroanal. Chem , 111 (1980) 105.
22 R Luther and F Pokorny, Z. Anorg. Allg. Chem , 57 (1908) 290.
23 L Young, Anodic Oxide Films, Academic Press, London, 1961, p 302.
24 J.P. Hoare, The Electrochemistry of Oxygen, Interscience, New York, 1968, p 211
25 N.A. Shumilova and G.V. Zhutaeva in A.J Bard (Ed), Encyclopedia of Electrochemistry of the Elements, Vol. 8, Marcel Dekker, New York, 1978, p 1
26 M Lopez Teijelo, J.R. Vilche and A.J Arvia, J. Electroanal. Chem , 131 (1982) 331

27 R.S. Schrebler Guzmán, J R Vılche and A J Arvía, Corros Scı , 18 (1978) 765
28 R. Córdova, M E. Martıns and A J. Arvía, J Electrochem Soc , 126 (1979) 1172
29 H. Angerstein-Kozlowska, B E. Conway, B. Barnett and J Mozota, J Electroanal Chem , 100 (1979) 417
30 R S. Schrebler Guzmán, J R Vılche and A J. Arvía, Electrochım Acta, 24 (1979) 395
31 M Y Duarte, M.E Martıns and A J Arvía, Electrochım. Acta, 25 (1980) 1613
32 R.S. Schrebler Guzmán, J R Vılche and A.J. Arvía, J Appl. Electrochem , 11 (1981) 551.
33 J.R. Vılche and A J. Arvía, Anal Acad Nac Cs Ex. Fıs. Nat , Buenos Aıres, 33 (1981) 33
34 H. Gomez Meıer, J.R Vılche and A J. Arvía, J Electroanal Chem , 134 (1982) 251
35 V.A Macagno and J R Vılche, Anal Acad. Nac Cs. Ex Fıs Nat , Buenos Aıres, ın press
36 H L Johnston, F. Cuta and A B Garret, J Am. Chem Soc., 55 (1933) 2311
37 E. Bosco and S K Rangarajan, J Electroanal. Chem , 129 (1981) 25, 134 (1982) 213, 225
38 C.C Busby and J.A Creıghton, J Electroanal Chem., 133 (1982) 183
39 G Lacconı, A S Gıoda and V A Macagno, Cong Argentıno Fısıcoquımıca, La Plata, Sept 1983
40 M.E. Martıns and A J Arvía, J Electroanal Chem , ın press.
41 M. Lopez Teıjelo, J.O Zerbıno, J R Vılche and A J Arvía, Electrochım Acta, submıtted